Actin turnover–dependent fast dissociation of capping protein in the dendritic nucleation actin network: evidence of frequent filament severing

Takushi Miyoshi,[1] Takahiro Tsuji,[1] Chiharu Higashida,[1] Maud Hertzog,[2,3] Akiko Fujita,[1] Shuh Narumiya,[1] Giorgio Scita,[2,3] and Naoki Watanabe[1]

[1]Department of Pharmacology, Kyoto University Faculty of Medicine, Sakyo-ku, Kyoto 606-8501, Japan
[2]Fondazione Italiana per la Ricerca sul Cancro Istituto di Oncologia Molecolare, 20139 Milan, Italy
[3]Department of Experimental Oncology, Istituto Europeo di Oncologia, 20141 Milan, Italy

Actin forms the dendritic nucleation network and undergoes rapid polymerization-depolymerization cycles in lamellipodia. To elucidate the mechanism of actin disassembly, we characterized molecular kinetics of the major filament end-binding proteins Arp2/3 complex and capping protein (CP) using single-molecule speckle microscopy. We have determined the dissociation rates of Arp2/3 and CP as 0.048 and 0.58 s^{-1}, respectively, in lamellipodia of live XTC fibroblasts. This CP dissociation rate is three orders of magnitude faster than in vitro. CP dissociates slower from actin stress fibers than from the lamellipodial actin network, suggesting that CP dissociation correlates with actin filament dynamics. We found that jasplakinolide, an actin depolymerization inhibitor, rapidly blocked the fast CP dissociation in cells. Consistently, the coexpression of LIM kinase prolonged CP speckle lifetime in lamellipodia. These results suggest that cofilin-mediated actin disassembly triggers CP dissociation from actin filaments. We predict that filament severing and end-to-end annealing might take place fairly frequently in the dendritic nucleation actin arrays.

Introduction

Migrating cells form a dynamic, thin, veil-like structure called lamellipodia at the leading edge. The dendritic nucleation model describes the reorganization processes of actin arrays in lamellipodia (Carlier et al., 2003; Pollard and Borisy, 2003). Within the lamellipodia, actin filaments display a branched network (Svitkina and Borisy, 1999). The Arp2/3 complex nucleates actin filaments off the sides of preexisting filaments (Mullins et al., 1998; Welch et al., 1998; Amann and Pollard, 2001; Fujiwara et al., 2002). Nucleated filaments elongate toward the leading edge (Small et al., 1978), and their growth is terminated by capping protein (CP; Mejillano et al., 2004; Wear and Cooper, 2004). Actin then depolymerizes to replenish the monomeric actin pool for the next round of polymerization. Quantitative modeling of the dendritic nucleation actin array is a logical goal in cell migration research, but it will require precise knowledge on the mechanisms governing actin filament turnover in vivo.

Our previous study using single-molecule speckle microscopy investigated actin filament lifetime distribution in lamellipodia of spreading *Xenopus laevis* fibroblasts (Watanabe and Mitchison, 2002). The filament lifetime spanned a wide range of time with a maximum of 148 s. Notably, one third of the filaments had a short lifetime of $<$10 s. This raised the question of what mechanisms may account for the observed lifetime of actin filaments.

In this study, we further extend our single-molecule speckle analysis to major actin end-binding proteins to elucidate the filament turnover mechanism. Single-molecule observations allow us to precisely measure the dissociation kinetics of a molecule in cells given that the molecule binds cellular structures on the order of seconds. Surprisingly, the dissociation of CP from actin was found to occur three orders of magnitude faster in cells than in vitro and even much faster than the actin disassembly rate. We demonstrate that the CP dissociation rate is prolonged under the several conditions in which actin filaments are stabilized. Our data indicate that

Correspondence to Naoki Watanabe: naoki-w@mfour.med.kyoto-u.ac.jp

Abbreviations used in this paper: CMV, cytomegalovirus; CP, capping protein; F-actin, filamentous actin; Jas, jasplakinolide; LIMK, LIM kinase; mRFP, monomeric red fluorescent protein; PLL, poly-L-lysine; SF, stress fiber.

The online version of this article contains supplemental material.

The Journal of Cell Biology, Vol. 175, No. 6, December 18, 2006 947–955
http://www.jcb.org/cgi/doi/10.1083/jcb.200604176

cofilin-mediated actin disassembly is required for the fast CP dissociation in lamellipodia. Based on the marked difference in the dissociation rate between actin (0.03 s^{-1}) and CP (0.58 s^{-1}), we predict that fairly frequent filament severing and end-to-end annealing might take place in the dendritic nucleation actin arrays.

Results

Fast dissociation kinetics of CP in lamellipodia

CP has been attributed to most of the actin capping activity in cell lysates (DiNubile et al., 1995; Hug et al., 1995) and has been found as an essential protein in the regulation of lamellipodium morphology (Rogers et al., 2003). Therefore, we analyzed the dynamics of CP to elucidate the state of barbed ends in the dendritic nucleation network. We generated three expression constructs by tagging either the α or β subunit of *Xenopus* CP with an EGFP. Of the three, two probes, EGFP-CPβ1 and CPβ1-EGFP, distributed to lamellipodia, which is consistent with previous studies (Schafer et al., 1998; Mejillano et al., 2004). EGFP-CPβ1 and CPβ1-EGFP speckles moved along with the retrograde actin flow, which suggested their association with actin structures (Fig. 1 A and Videos 1 and 2, available at http://www.jcb.org/cgi/content/full/jcb.200604176/DC1). We selected these two probes for single-molecule speckle analysis of CP.

We measured the lifetime distribution of single-molecule CP speckles in lamellipodia of XTC cells spreading on poly-L-lysine (PLL)–coated glass coverslips. EGFP-CPβ1 and CPβ1-EGFP showed a similar lifetime distribution (Fig. 1, B and C). Our measurement revealed that 53–60% of CP dissociated from actin within 1 s. When the CP lifetime distribution was fit with a single exponential curve, the half-life was 1.20 and 1.23 s for EGFP-CPβ1 and CPβ1-EGFP, respectively, which is in marked contrast to the slow dissociation of CP from barbed ends in vitro ($t_{1/2}$ = ∼28 min; Schafer et al., 1996). CP displayed similar lifetime distributions throughout lamellipodia (Fig. 1 D).

We next examined the spatial location of CP recruitment. We recorded positions of newly appearing CP speckles and measured the distance from the cell edge. Although CP speckles appeared most frequently in the tip region, appearance was widely distributed throughout the lamellipodia (Fig. 1 E). This bias toward the lamellipodium tip region was weaker than that observed for the Arp2/3 complex (see Fig. 3 E).

Given this unexpectedly fast dissociation, we needed to test whether our EGFP-tagged CP probes retained high affinity to barbed ends. We characterized biochemical properties of the recombinant CPα2/EGFP-CPβ1 heterodimer expressed in *Escherichia coli* (Fig. 2 A). First, we determined the on-rate constant (k_{on}) of CPα2/EGFP-CPβ1 using a pyrene-actin polymerization assay (Fig. 2 B). Low concentrations of CPα2/EGFP-CPβ1 efficiently inhibited barbed end elongation from filamentous actin (F-actin) seeds. The on-rate constant was calculated to be 3.9 $\mu M^{-1}s^{-1}$, which was comparable with that of native CP (3.5–5.7 $\mu M^{-1}s^{-1}$; Schafer et al., 1996). Second, we measured the dissociation constant (K_d) using a pyrene-actin steady-state assay (Fig. 2 C). The K_d of CPα2/EGFP-CPβ1 with barbed ends was 1.3 nM, which was comparable with the K_d of native CP (0.06–1 nM; Caldwell et al., 1989; Casella and Torres, 1994; Schafer et al., 1996). The K_d and on-rate constant predict an off-rate constant of 5.1 × 10^{-3} s^{-1}, which is ∼100-fold smaller than the dissociation rate of our CP probes in lamellipodia (Fig. 1, B and C). We also noted that recombinant EGFP-CPβ1, which was expressed and purified in the absence of CPα subunits, did not interfere with actin elongation (unpublished data). This is consistent with previous findings (Casella and Torres, 1994). Therefore, CP speckles observed in cells should correspond to EGFP-CPβ1 coupled with endogenous CPα subunits but not deficient EGFP-CPβ1 monomers.

To further evaluate the fidelity of our CP probes, we permeabilized cells expressing EGFP-CPβ1 using Triton X-100 and followed the decay of EGFP fluorescence. The decay rate of fluorescence intensity was 1.7 × 10^{-4} s^{-1} in lamellipodia

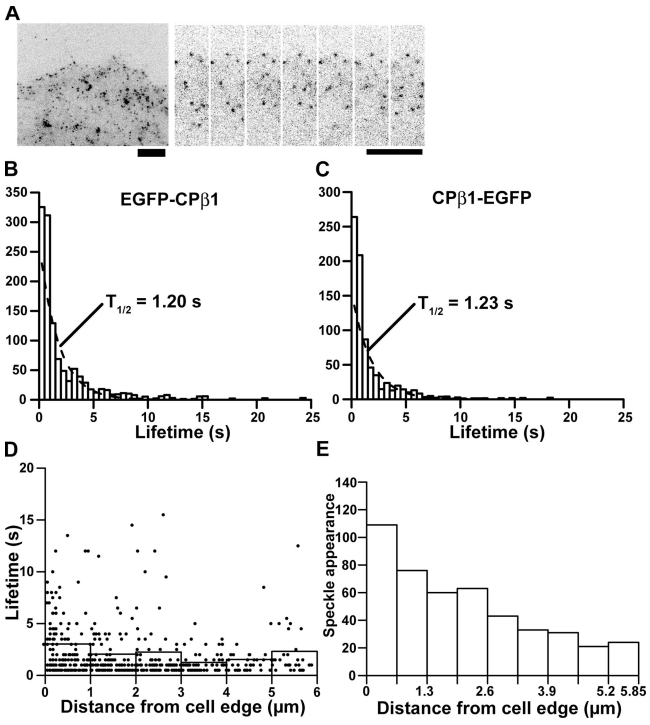

Figure 1. **Lifetime distribution of single-molecule CP speckles in lamellipodia.** (A) Speckle images in an XTC cell expressing a low amount of EGFP-CPβ1 (left) and associated time-lapse images at intervals of 500 ms (right). (B and C) Speckle lifetime distribution of EGFP-CPβ1 (n = 1,195) in two cells (B) and CPβ1-EGFP (n = 793) in three cells (C). CP speckles with single EGFP intensity, which appeared over the course of a 15-s time window, were followed. Bars show the number of speckles with indicated lifetimes after normalization for photobleaching. Dashed lines show the single exponential curve fit with lifetime distribution data between 1.0 and 5.5 s, and its decay rate is expressed as half-life ($t_{1/2}$). (D) Lifetime versus position plot of CP speckle lifetime data. Dots represent the lifetime and emerging position of individual EGFP-CPβ1 speckles. Bars represent the mean speckle lifetime after correction for photobleaching. A representative result of two independent measurements is shown. (E) The position of EGFP-CPβ1 speckles that had appeared over 30 consecutive images was recorded. Bars represent the number of newly emerged CP speckles in each indicated position. A representative result of three independent measurements is shown. Bars, 5 μm.

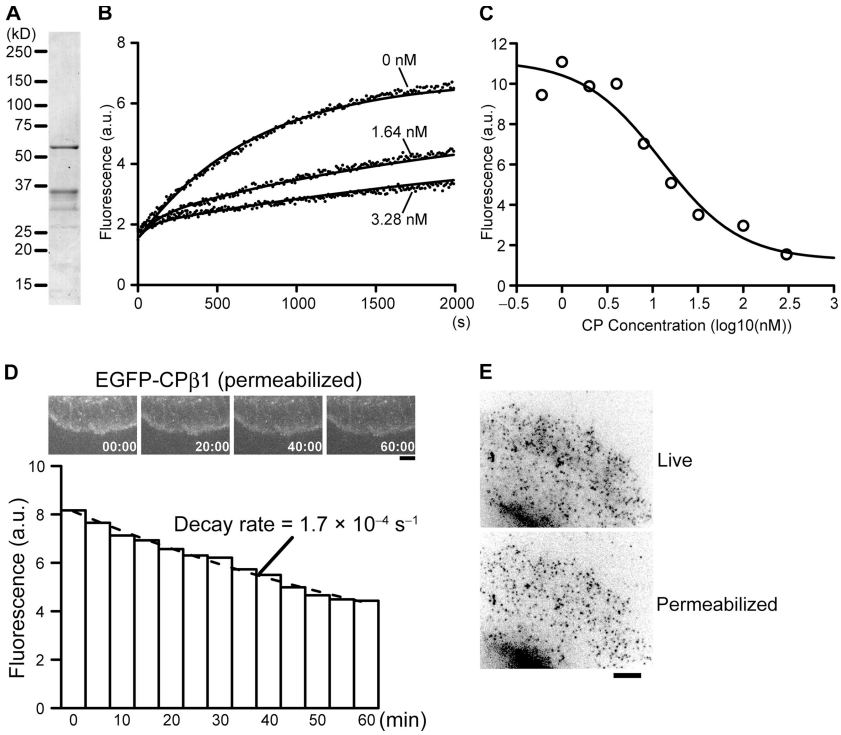

Figure 2. **Verification of EGFP-tagged CP probes.** (A) CPα2/EGFP-CPβ1 heterodimer purified from *E. coli* stained with Coomassie Brilliant blue. Numbers indicate the molecular mass in kilodaltons. (B) Effect of recombinant CPα2/EGFP-CPβ1 on actin polymerization from F-actin seeds. The change in pyrene-actin (1 μM) fluorescence after simultaneous mixing with preformed F-actin seeds and indicated concentrations of CPα2/EGFP-CPβ1 is plotted. Solid lines show the curves predicted from kinetic modeling of actin polymerization at the CP on rate of 3.9 $\mu M^{-1}s^{-1}$ and the CP off rate of 1.9×10^{-3} s^{-1}. (C) Change in steady-state pyrene-actin fluorescence with varying concentrations of CPα2/EGFP-CPβ1 (circles). The line shows the curve optimized for fluorescence data (circles), which was calculated using 1.3 nM for K_d between CP and barbed ends. (D) Slow dissociation of EGFP-CPβ1 after permeabilization. Cells expressing EGFP-CPβ1 were permeabilized with 0.1% Triton X-100 in CB for 10 s, and time-lapse images were acquired in a buffer (10 mM Hepes, pH 7.4, 100 mM KCl, 2 mM $MgCl_2$, 0.2 mM EGTA, and 1 mM DTT; top). Time is given in minutes and seconds. Graph shows the fluorescence intensity of EGFP-CPβ1. Dashed line shows the single exponential curve fit with fluorescence data, which gives the decay rate of 1.7×10^{-4} s^{-1}. (E) Preservation of EGFP-CPβ1 speckles during the permeabilization procedure. The top and bottom images show EGFP-CPβ1 speckles in an XTC cell before and after permeabilization, respectively, performed as in D. The loss of EGFP-CPβ1 signals between two images as a result of photobleaching is ~15%. Bars, 5 μm.

(Fig. 2 D). Cells retained most of the expressed CP speckles during the permeabilization procedure (Fig. 2 E), eliminating the possibility that our permeabilization procedure selected a specific fraction of CP tightly bound to actin. These results indicate that our CP probes bind barbed ends with a high affinity, similar to that measured for unmodified protein in vitro (Caldwell et al., 1989; Casella and Torres, 1994; Schafer et al., 1996). All together, our CP probes can be used as a reliable marker to monitor the dynamics of CP. We conclude that fast dissociation kinetics of CP speckles represent the dynamics of endogenous CP.

To test whether other barbed end interactors might cap actin tightly, we visualized the molecular dynamics of Eps8, VASP, and gelsolin (Fig. S1 and Videos 3–7, available at http://www.jcb.org/cgi/content/full/jcb.200604176/DC1; Witke et al., 1995; Bear et al., 2002; Croce et al., 2004; Disanza et al., 2004; Barzik et al., 2005). None of the three molecules displayed long-term association with the actin network. These results suggest that the majority of actin filaments may release barbed end cappers and revert to the growing phase quickly in lamellipodia.

Kinetics of the Arp2/3 complex in lamellipodia

We next examined the molecular dynamics of the Arp2/3 complex in lamellipodia. We generated expression constructs by tagging each of seven *Xenopus* Arp2/3 subunits with EGFP, testing N- and C-terminal fusions in several cases. Among them, four probes— EGFP-p40, p40-EGFP, EGFP-p21, and p21-EGFP—were localized to lamellipodia and cytoplasmic punctate actin structures, which is consistent with the reported Arp2/3 localization (Mullins et al., 1997; Welch et al., 1997; Schafer et al., 1998; Svitkina and Borisy, 1999). Using an anti-p40 antibody, we confirmed that distributions of EGFP-p21 and p21-EGFP were identical to that of the endogenous p40 subunit of Arp2/3 (Fig. S2, available at http://www.jcb.org/cgi/content/full/jcb.200604176/DC1). We also compared localization of the four probes with each other by generating probes tagged with monomeric red fluorescent protein 1 (mRFP1; Campbell et al., 2002). All four probes showed identical localization (Fig. S2) and moved inward at the same rate as the retrograde actin flow. Based on these observations, we selected these four probes for further analysis.

We analyzed the kinetics of Arp2/3 dissociation from the actin network in lamellipodia. We followed each newly emerged single-molecule Arp2/3 speckle and measured the duration between its appearance and disappearance (Fig. 3, A–D; and Video 8, available at http://www.jcb.org/cgi/content/full/jcb.200604176/DC1). Arp2/3 interacts with the side of actin filaments with micromolar affinity (Mullins et al., 1997; Gournier et al., 2001). Thus, Arp2/3 is expected to dissociate from the side of the filament on a subsecond timescale after leaving the pointed end, and rapidly dissociating side binding would not be detected using our current experimental settings. Therefore, we interpret that the lifetime of Arp2/3 speckles represents the duration of Arp2/3 association with the pointed end, although we do not know whether Arp2/3 dissociation occurs simultaneously with debranching. The lifetime distribution of Arp2/3 speckles could be approximated by a single exponential curve, which suggests that the dissociation of Arp2/3 is governed by a single rate-limiting step. Half-life determined for four Arp2/3 probes yielded similar values that spanned 12.5 to 16.9 s. The half-life of Arp2/3 speckles is about half of

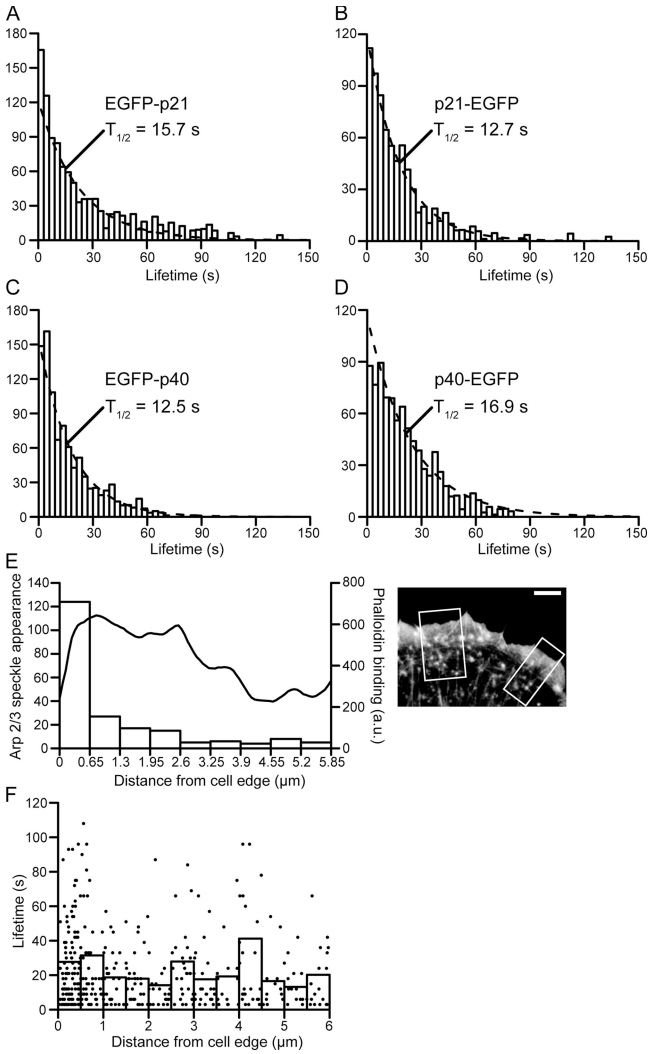

Figure 3. **Lifetime distribution of single-molecule Arp2/3 complex speckles in lamellipodia.** (A–D) Speckle lifetime distribution of EGFP-p21 (n = 1088; A), p21-EGFP (n = 736; B), EGFP-p40 (n = 955; C), and p40-EGFP (n = 865; D) in two cells in the lamellipodia of XTC cells spreading on PLL-coated glass coverslips. Arp2/3 speckles with single-molecule EGFP fluorescence intensity that appeared over the course of a 90-s time window were followed in each analysis. Bars show the number of speckles with the indicated lifetime after correction for photobleaching. Dashed lines show the single exponential curve fit with data between 6 and 48 s, and its decay rate is expressed as half-life ($t_{1/2}$). (E) Images of EGFP-p40 speckles were acquired at intervals of 3 s, and cells were fixed and stained with phalloidin (right). The areas devoid of dense clusters of speckles (boxed areas; right) were chosen for analysis. The position of Arp2/3 speckles that had appeared over 30 consecutive images (n = 214) was recorded. The curve represents the actin filament distribution measured by phalloidin binding. Bars represent the number of newly emerged Arp2/3 speckles in each indicated position. A representative result of two independent measurements is shown. Bar, 5 μm. (F) Lifetime versus position plot of Arp2/3 speckle lifetime data. Dots represent the lifetime and emerging position of individual EGFP-p21 speckles (n = 516). Bars represent the mean speckle lifetime after correction for photobleaching. A representative result of four independent measurements is shown.

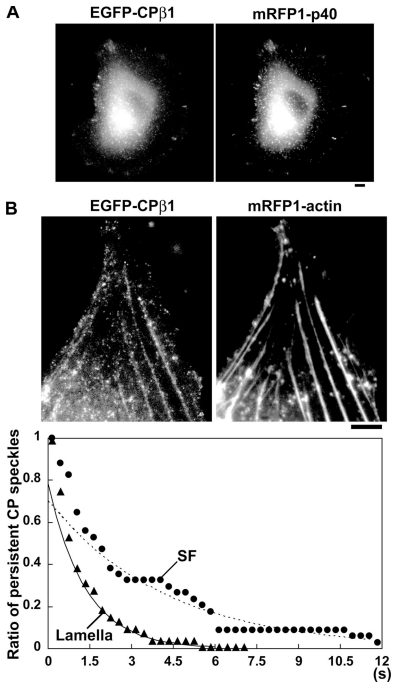

Figure 4. **Slower dissociation kinetics of CP associated with actin SFs.** (A) Colocalization of CP and Arp2/3 at the leading edge and cytoplasmic punctate actin structures in a spreading XTC cell. A live XTC cell expressing EGFP-CPβ1 (left) and mRFP1-p40 (right) 2 h after seeding onto a PLL-coated glass coverslip. (B) Association of CP with actin stress fibers (SF). A live XTC cell expressing EGFP-CPβ1 (top left) and mRFP1-actin (top right) 4.5 h after seeding onto a PLL-coated glass coverslip. The graph shows decay in the number of persistent EGFP-CPβ1 speckles located on SFs (circles) and in the lamella area away from SFs (triangles) in the same cell. Lines: the single exponential curve fit gives 2.9 and 0.95 s for the half-life of CP on SFs (dotted) and away from SFs (solid), respectively, after normalization for photobleaching. A representative result of two measurements is shown. Bars, 5 μm.

that of actin filaments in lamellipodia of XTC cells (Watanabe and Mitchison, 2002).

Next, we examined the spatial location of Arp2/3 recruitment by recording positions of newly appearing speckles. Although Arp2/3 speckles appeared throughout lamellipodia, appearance was heavily biased to a zone within 0.5 μm from the cell edge (Fig. 3 E). This bias was greater than that previously observed for actin speckles (Watanabe and Mitchison, 2002) and suggests that most Arp2/3-driven nucleation occurs in the tip region of the leading edge, where known Arp2/3 activators are localized (Nakagawa et al., 2001). The mean lifetime of Arp2/3 did not change throughout lamellipodia, although Arp2/3 with prolonged lifetime was observed more frequently in the cell edge region than in the rest of lamellipodia (Fig. 3 F).

Less dynamic behavior of CP bound to actin stress fibers

Under our normal observation conditions, up to 2 h after cells were seeded on PLL-coated coverslips, our CP probes were predominantly colocalized with Arp2/3 in lamellipodia and cytoplasmic punctate actin structures (Fig. 4 A). When cells were allowed to grow for another several hours, CP probes were also associated with actin stress fibers (SFs; Fig. 4 B). The similar localization of CP to myofibrillar structures in cultured cardiomyocytes has been reported previously (Schafer et al., 1994). We noticed that a fraction of CP speckles stayed stably associated with SFs, whereas CP speckles that did not localize with

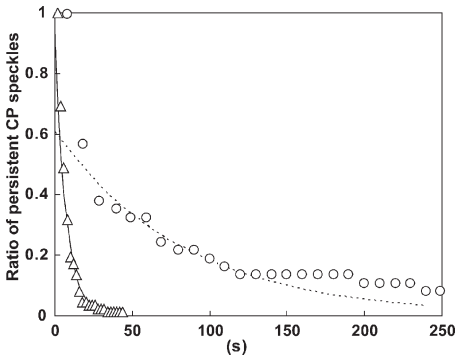

Figure 5. **Rapid, marked stabilization of CP upon Jas treatment.** Images of EGFP-CPβ1 speckles in live XTC cells were acquired at 2-s intervals before perfusion and at 10-s intervals 1 min after the perfusion of 1 μM Jas. The decay of persistent single-molecule CP speckles before (circles) and ∼1–5 min after (triangles) perfusion is shown. The normalized half-life of persistent CP speckles rapidly increased from 4.26 (solid line) to 68.9 s (dotted line) upon Jas treatment. A representative result of three measurements is shown.

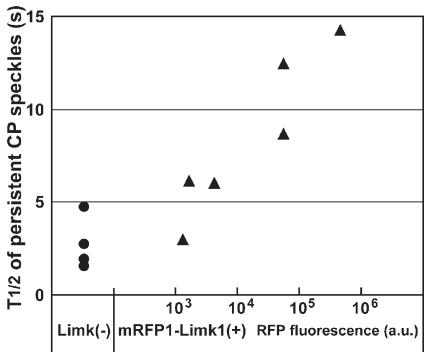

Figure 6. **The dissociation rate of CP speckles is reduced by coexpression of LIMK.** XTC cells were transfected with various ratios of the mixture of delCMV-EGFP-CPβ1 and pmRFP1–hLIMK-1 and were allowed to spread on PLL-coated coverslips for 0.5–2 h. Circles show the half-life of single-molecule CP speckles in lamellipodia of cells (n = 4) transfected with delCMV-EGFP-CPβ1 alone. The half-life of single-molecule CP speckles in lamellipodia and the total RFP fluorescence intensity in individual cells were plotted (triangles).

SFs in the lamella region emerged and disappeared as quickly as in lamellipodia. When subjected to speckle regression analysis (Watanabe and Mitchison, 2002), the decay rate of persistent CP speckles located on SFs was slower than that of CP in the other area of lamella (Fig. 4 B). These results suggest that CP dissociation is differentially regulated in distinct actin structures and that the dissociation rate of CP may be correlated with the actin filament turnover rate.

Attenuation of fast CP dissociation by the inhibition of actin disassembly

Next, we examined the effect of stabilization of actin filaments on the dissociation kinetics of CP. We tested jasplakinolide (Jas), an actin depolymerization inhibitor (Bubb et al., 2000) that induces a three- to fourfold increase in the half-life of actin filaments within 1 min in lamellipodia (Watanabe and Mitchison, 2002). We observed a rapid, marked prolongation of CP speckle lifetime upon treatment with 1 μM Jas (Fig. 5 and Video 9, available at http://www.jcb.org/cgi/content/full/jcb.200604176/DC1). This finding is striking, as the half-life of actin filament turnover (∼30 s; Watanabe and Mitchison, 2002) greatly (∼20-fold) exceeds that of CP, and it is a counterintuitive phenomenon that inhibiting the disassembly of a network system has a strong impact on the kinetics of its associated molecule, which displays much faster binding-dissociation kinetics.

To confirm this, we tested whether the inactivation of cofilin, a major actin depolymerizing factor implicated in lamellipodium formation (Bamburg, 1999; Chan et al., 2000; Nagata-Ohashi et al., 2004), may also have similar effects. LIM kinase (LIMK) phosphorylates cofilin and prevents the interaction between cofilin and actin (Yang et al., 1998). We generated an expression construct for mRFP1-tagged human LIMK (mRFP1–hLIMK-1) to examine the effect of various levels of LIMK-1 expression on CP. It was confirmed that cells expressing mRFP1–hLIMK-1 displayed slower actin filament turnover (Fig. S3 and Video 10, available at http://www.jcb.org/cgi/content/full/jcb.200604176/DC1), which is consistent with previous findings (Hotulainen et al., 2005). The decay rate of persistent CP speckles in lamellipodia was also markedly prolonged in cells expressing mRFP1–hLIMK-1, and this effect was correlated with the expression level of mRFP1–hLIMK-1 (Fig. 6). These results indicate that cofilin-mediated actin disassembly is responsible for the fast dissociation kinetics of CP in lamellipodia. Because three different conditions of actin filament stabilization led to the prolongation of CP speckle lifetime (Figs. 4–6), filament severing may frequently take place in lamellipodia, which could lead to the fast dissociation of CP from the actin network.

Discussion

This study reveals the astoundingly fast dissociation kinetics of CP in lamellipodia. In vitro, native CP binds barbed ends with subnanomolar affinities, and CP dissociates from barbed ends at a very slow rate (∼0.0004 s^{-1}; Caldwell et al., 1989; Casella and Torres, 1994; Schafer et al., 1996). In contrast, our CP probes displayed three orders of magnitude faster dissociation kinetics in cells. Several studies have already suggested the weak interaction of CP with barbed ends in cell lysates. Nearly 1 μM of free barbed ends are present despite ∼1–2 μM CP being present in lysates obtained from *Dictyostelium discoideum* cells (Hug et al., 1995) and neutrophils (DiNubile et al., 1995). The dissociation constant of CP in cell lysates was estimated to be ∼0.1 μM (Hug et al., 1995). The weak affinity of CP to barbed ends has now been confirmed by our data obtained using intact cells. Moreover, our results conclude that the fast dissociation of CP, but not its slow association as postulated (Hug et al., 1995), is responsible for the weak capping activity. Attenuation of the fast dissociation of CP probes upon permeabilization can be explained by the removal of CP dissociation promoters such as phosphatidylinositol bisphosphate (Schafer et al., 1996) and CARMIL (Yang et al., 2005). An unidentified anti-CP factor that differs from VASP and CARMIL has also been reported previously (Huang et al., 2005).

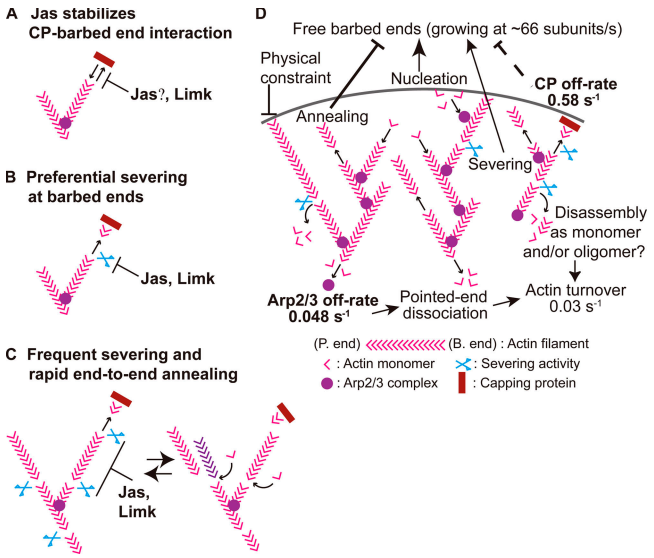

Figure 7. **Models for actin dynamics–dependent fast CP dissociation and filament turnover kinetics in the dendritic nucleation actin arrays.** (A) Direct inhibition of CP dissociation by Jas. Jas might stabilize the CP–barbed end interaction through conformational changes in the filament, and cofilin might have the opposite effect. (B) Preferential filament severing near the barbed end. Both models (A and B) predict an unknown barbed end–specific regulation in the mechanism of cofilin-mediated actin disassembly. (C) Alternatively, filament severing might occur at a high frequency. In this model, end-to-end annealing will be required to prevent fast actin disassembly and uncontrolled growth of free barbed ends. Because CP dissociates one order of magnitude faster than actin and Arp2/3, this model predicts that severing may occur several times in a single filament before disassembly. (D) Summary of the kinetics of actin filament turnover regulation. The present single-molecule speckle analysis revealed 0.048 and 0.58 s^{-1} for the dissociation rates of Arp2/3 and CP, respectively. We have also reevaluated the speed to the FH2 mutant of mDia1 in lamellipodia and determined the growth rate of free barbed ends as ~66 subunits/s (Fig. S5, available at http://www.jcb.org/cgi/content/full/jcb.200604176/DC1). Thus, the growth of barbed ends is not strictly limited by capping, whereas disassembly from the Arp2/3-bound pointed ends starts slowly. Therefore, we predict that filament severing is required to achieve fast actin disassembly in lamellipodia. End-to-end filament annealing probably contributes to the neutralization of free barbed ends generated by nucleation and severing. Our data also predict that CP as well as a fraction of actin may dissociate from the network as small actin oligomers.

Twinfilin, a barbed end–interacting protein with a G-actin sequestering activity (Helfer et al., 2006), interacts directly with CP without affecting the interaction of CP with barbed ends (Falck et al., 2004). These molecules may contribute to the fast dissociation of CP. However, based on our findings of the strong dependency of the CP dissociation rate on actin filament turnover (Figs. 4–6), we propose that cofilin-mediated filament severing may trigger the dissociation of CP from the dendritic nucleation actin arrays.

Possible mechanisms for actin filament turnover–dependent CP dissociation are depicted in Fig. 7 (A–C). Jas might strengthen CP–actin interaction by affecting filament conformation (Fig. 7 A). However, because CP alone can bind F-actin with a very high affinity, further stabilization of CP–barbed end interaction by Jas seems questionable.

Alternatively, filament severing induced by cofilin may possibly trigger the dissociation of CP attached to a small actin oligomer. Jas, which binds actin filaments competitively with phalloidin (Bubb et al., 1994), probably exerts antisevering effects in a similar manner to phalloidin. If filament severing by cofilin triggers fast CP dissociation, there must be a mechanism that prevents the actin network from equally fast breakdown. Disassembly of actin filaments ($t_{1/2}$ = 30 s; Watanabe and Mitchison, 2002) is ~20-fold slower than the dissociation of CP in lamellipodia of XTC cells. One possible explanation is that cofilin may sever actin filaments preferentially near the barbed end (Fig. 7 B). Another possibility is that cofilin-mediated severing occurs frequently throughout the actin arrays, and rapid end-to-end annealing may prevent severed actin oligomers from leaving the filament network (Fig. 7 C). In vitro, rapid reannealing of sheared actin filaments has long been recognized (Nakaoka and Kasai, 1969; Carlier et al., 1984; Andrianantoandro et al., 2001). Annealing appears to be a favorable reaction given the high density of actin filaments, which is ~1,000 μM in lamellipodia (Abraham et al., 1999). To gain evidence for filament annealing, we examined the distribution of free filament ends using recombinant EGFP-tagged CP and tropomodulin (Weber et al., 1994) in permeabilized XTC cells. From the binding density of these fluorescent probes to lamellipodia, the concentrations of free barbed ends and pointed ends were estimated to be 0.99 and 4.6 μM, respectively (Fig. S4, available at http://www.jcb.org/cgi/content/full/jcb.200604176/DC1). The coexistence of high amounts of free barbed ends and pointed ends may support our hypothesis of frequent end-to-end filament annealing (Fig. 7 C).

The current dendritic nucleation models did not incorporate end-to-end filament annealing as a dominant reaction because CP has been believed to terminate barbed end growth within 1–2 s after the nucleation of filaments (Carlier et al., 2003; Pollard and Borisy, 2003). Now, our finding of fast CP dissociation suggests that CP is not sufficient to strictly block barbed ends in lamellipodia. The present study also tested whether other molecules exist that are capable of tightly capping a major fraction of filaments. Gelsolin$^{-/-}$ fibroblasts display a reduced membrane ruffling response to EGF (Witke et al., 1995; Azuma et al., 1998). Eps8$^{-/-}$ fibroblasts are defective in membrane ruffling formation induced by PDGF (Scita et al., 1999), and *Caenorhabditis elegans* lacking Eps8 displays severe defects in the organization of intestinal brush border microvilli (Croce et al., 2004). However, our data show that none of these barbed end factors, including gelsolin, Eps8, and VASP, cap actin tightly in lamellipodia. Notably, the dissociation constant of Eps8 with barbed ends determined in vitro (Disanza et al., 2004) was also considerably lower than that observed in vivo. Collectively, these results suggest that free barbed ends are abundant in lamellipodia despite these cappers, whose affinities to barbed ends are within the nanomolar range in vitro. Our findings of the fast dissociation kinetics of these cappers from the actin network have opened up a possibility that end-to-end filament annealing may ubiquitously occur in lamellipodia.

Fig. 4 D summarizes kinetics in regulation of the dendritic nucleation actin arrays. Our single-molecule speckle analysis revealed 0.048 and 0.58 s^{-1} for the dissociation rates of Arp2/3 and CP, respectively. Another important notion is the fast actin

elongation in living cells as revealed by the actin polymerization–driven movement of mDia1 (Higashida et al., 2004). Based on the speed of mDia1F2 (Fig. S5, available at http://www.jcb.org/cgi/content/full/jcb.200604176/DC1), we estimate that free barbed ends may elongate at ~66 subunits/s in lamellipodia. Together with the fast dissociation kinetics of CP, these results suggest that barbed end growth is not strictly restricted as previously postulated. Given the relatively free and fast barbed end growth, we also predict the requirement of filament severing in catalyzing the fast actin disassembly in lamellipodia based on kinetic modeling (unpublished data). Filament severing is also relevant, as it seems indispensable to facilitate fast actin turnover (Theriot and Mitchison, 1991; Watanabe and Mitchison, 2002) in the presence of actin filaments of several microns in length found in lamellipodia (Small et al., 1995).

Collectively, we predict that filament severing and its counteracting reaction, end-to-end annealing, may take place frequently in lamellipodia. Filament severing and end-to-end annealing could play a pivotal role in leading edge dynamics by rapidly changing the direction of growth, length distribution, disassembly, and polarity of the actin filament arrays. Currently, it is difficult to estimate the frequency of these two inverse reactions in cells. However, our finding of the fast CP dissociation kinetics may imply a severing frequency of up to one per second for an actin filament of several tens of subunits in length. Further studies will be required to test this high frequency severing-annealing hypothesis.

Materials and methods

Plasmids and reagents

EST clones encoding subunits of *Xenopus* Arp2/3, CP, and other actin-related proteins were obtained from the IMAGE consortium. GenBank/EMBL/DDBJ accession no. for sequence data are as follows: EF011871 (Arp3), EF011865 (Arp2), EF011872 (p40), EF011864 (p34), EF011866 (p21), EF011870 (p20), EF011868 (p16), BC060481 (CPα1), BC072853 (CPα2), EF011869 (CPβ1), BC072836 (VASP), BC084059 (gelsolin), and EF011867 (tropomodulin). Each cDNA was subcloned into the pEGFP-C1 (CLONTECH Laboratories, Inc.)–derived vector harboring the defective cytomegalovirus (CMV) promoter (Watanabe and Mitchison, 2002) delCMV-EGFP-C1. mRFP1 fusion constructs were generated by replacing EGFP sequences with mRFP1 cDNA (gift from R.Y. Tsien, University of California, San Diego, San Diego, CA; Campbell et al., 2002). Full-length pEGFP-Eps8 was described previously (Scita et al., 2001). pmRFP1–hLIMK-1 was constructed by introducing wild-type human LIMK-1 cDNA (gift from K. Mizuno, Tohoku University, Sendai, Japan; Yang et al., 1998) into the mRFP1 expression vector. Jas was purchased from Calbiochem.

Antibody and immunocytochemistry

The guinea pig anti-p40 antibody was raised against the 6xHis-tagged p40 subunit using pET-30a (Novagen). For immunocytochemistry, cells were extracted with 0.1% Triton X-100 in Cytoskeleton buffer (CB; 10 mM MES, pH 6.1, 90 mM KCl, 3 mM $MgCl_2$, 2 mM EGTA, and 0.16 M sucrose) for 10 s and fixed with 3.7% PFA in CB for 20 min at room temperature. Texas red–X phalloidin (Invitrogen) was used for staining F-actin. AlexaFluor488 and -594 anti–guinea pig IgG (Invitrogen) were used as secondary antibodies.

Live cell imaging and fluorescent speckle microscopy

Speckle imaging was performed as described previously (Watanabe and Mitchison, 2002). In brief, cells were allowed to spread on a PLL-coated glass coverslip attached to a flow cell in 70% Leibovitz's L15 medium (Invitrogen) without serum. The flow cell was placed on the stage of a microscope (BX52 or IX71; Olympus) equipped with either 100-W mercury or 75-W Xenon illumination and with a cooled CCD camera (MMX1300-YHS, CoolSNAP HQ, or Cascade II:512; Roper Scientific; or UIC-QE; Molecular Devices). Time-lapse imaging was performed at 21–23°C using MetaMorph software (Universal Imaging Corp.) up to 120 min after cells were seeded. Fluorescent speckle microscopy was performed by observing cells expressing a low amount of EGFP-tagged proteins using a planApo 100× NA 1.40 oil objective (Olympus). A restricted area near the cell edge was illuminated. Speckle lifetime measurement was performed by tracking individual speckles manually. The photobleaching rate of EGFP probes was measured by illuminating entire cell areas under an identical condition on the day of each experiment. Normalization for photobleaching was described previously (Watanabe and Mitchison, 2002).

Decay rate measurement of CP probes in permeabilized cells

XTC cells expressing EGFP-CPβ1 or CPβ1-EGFP were permeabilized with 0.1% Triton X-100 in CB for 10 s, and the medium was replaced with a buffer (10 mM Hepes, pH 7.4, 100 mM KCl, 2 mM $MgCl_2$, 0.2 mM EGTA, and 1 mM DTT). Time-lapse images were acquired at intervals of 5 min. Illumination was attenuated using neutral density filters so that fluorescence decay caused by photobleaching was negligible. EGFP fluorescence intensity was measured in a cell peripheral region after the subtraction of background values obtained in an area outside of the cell.

Purification of the recombinant CPα2/EGFP-CPβ1 heterodimer

pGEX-CPα2 was generated by inserting CPα2 cDNA into pGEX-2T (GE Healthcare). pET-30-EGFP-CPβ1 was generated by replacing 6xHis sequences in pET-30a (Novagen) with the EGFP-CPβ1 coding sequences. Using electroporation, BL21 Star (DE3; Invitrogen) harboring the pG-KJE8 chaperon plasmid (Takara) was transformed with pGEX-CPα2 and pET-30-EGFP-CPβ1 simultaneously. Subsequent cultures were performed under the selection pressure of ampicillin, kanamycin, and chloramphenocol.

Cells were grown at 37°C in Luria-Bertani medium overnight. After subculturing into fresh media, chaperon proteins were induced, and, at OD_{600} = 0.6, 1 mM IPTG was added. Cells were cultured at 30°C for an additional 6 h and collected by centrifugation. Cells were then sonicated in buffer C (10 mM Tris-Cl, pH 7.5, 300 mM NaCl, 1 mM $MgCl_2$, 1 mM DTT, and 1 mM ATP) supplemented with 0.5% Triton X-100, 200 μM PMSF, 2 μg/ml leupeptin, and 1 μg/ml pepstatin A. The sonicate was clarified by centrifugation. The supernatant was incubated with glutathione–Sepharose 4B (GE Healthcare), and the beads were washed by repeated centrifugation with buffer C. The beads were incubated with thrombin (Sigma-Aldrich) in buffer C, and CPα2/EGFP-CPβ1 cleaved from GST was collected in the supernatant. Thrombin activity was neutralized with hirudin (Sigma-Aldrich).

Pyrene-actin polymerization assay

Pyrene-labeled actin and rabbit skeletal muscle actin were purchased from Cytoskeleton, Inc. Before use, the protein concentrations were verified using densitometry on the SDS-PAGE gel stained with Coomassie Brilliant blue. Unlabeled actin was polymerized at 5 μM in buffer F (10 mM Tris-Cl, pH 7.5, 100 mM KCl, 2 mM $MgCl_2$, 1 mM ATP, 0.2 mM EGTA, and 0.2 mM DTT) for 1 h. For assembly from F-actin seeds, a 12.5-μl aliquot of unlabeled, preassembled actin filaments was inserted into each well. To start the reaction, 6.67 μl of a 15-μM pyrene-actin droplet in buffer G containing 0.2 mM ATP was washed into the F-actin seeds with 71 μl of 1.2× buffer F and 10 μl of buffer C containing a range of concentrations of CPα2/EGFP-CPβ1. Pyrene fluorescence was monitored at room temperature using Fluoroskan Ascent FL (Labsystems).

Determination of rate constants of the CPα2/EGFP-CPβ1 heterodimer

The rate constants for capping barbed ends were determined from kinetic parameter optimization using data collected in actin polymerization assays. The concentration of F-actin seeds, $[S]_0$, was first determined by fitting the fluorescence data without CPα2/EGFP-CPβ1 with the equation

$$[A_{Poly}] = ([A_{Free}]_0 - \frac{B_{off} + P_{off}}{B_{on} + P_{on}})(1 - e^{-(B_{on}+P_{on})[S]_0 t}),$$

where $[A_{Poly}]$ is the concentration of polymerized actin, $[A_{Free}]_0$ is the initial concentration of free actin monomers, B_{on} and B_{off} are on and off rates of barbed ends, and P_{on} and P_{off} are on and off rates of pointed ends.

Polymerization in the presence of CPα2/EGFP-CPβ1 is described as B + A_{Free} = B, B + C = BC, and P + A_{Free} = P, where A_{Free} is free actin monomers, B is free barbed ends, P is free pointed ends, C is free CP, and BC is capped barbed ends. Using $[S]_0$, actin polymerization curves

were calculated numerically by Euler's method. The on and off rates of CPα2/EGFP-CPβ1 were varied to fit calculated polymerization curves with pyrene-actin fluorescence data.

Determination of the dissociation constant (K_d) of CPα2/EGFP-CPβ1 heterodimer

2 μM pyrene-labeled actin was polymerized for 2 h in buffer F. Various amounts of CPα2/EGFP-CPβ1 in 10 μl of buffer C was added to 90 μl of the polymerized pyrene-actin solutions. Samples were incubated for 24 h at 22°C, and pyrene fluorescence was measured. At steady state,

$$B_{on}[B][A_{Free}] + P_{on}[P][A_{Free}] = B_{off}[B] + P_{off}[P] \text{ and } K_d = \frac{[B][C]}{[BC]},$$

where $[A_{Free}]$ is the concentration of free actin monomers, [B] is the concentration of free barbed ends, [P] is the concentration of free pointed ends, [C] is the concentration of free CP, and [BC] is the concentration of capped barbed ends.

At CP concentrations of ≥1 nM, the concentration of free CP, [C], is almost equal to its total concentration, $[C]_0$. The concentration of polymerized actin is calculated by the following equation:

$$[A_{Poly}] = [A_{Free}]_0 - \frac{B_{off}X + P_{off}}{B_{on}X + P_{on}}, \text{ where } X = \frac{K_d}{K_d + [C]_0}.$$

The K_d for CPα2/EGFP-CPβ1 was determined by optimizing this equation to fluorescence data.

Online supplemental material

Fig. S1 shows the fast dissociation of barbed end–interacting proteins Eps8 and VASP from the actin network in lamellipodia. Fig. S2 shows a comparison of the localization of our Arp2/3 constructs and endogenous Arp 2/3 in XTC cells. Fig. S3 shows reduced actin filament turnover in cells overexpressing LIMK. Fig. S4 shows the distribution of free barbed ends and pointed ends in permeabilized XTC cells visualized by recombinant CPα2/EGFP-CPβ1 and GST-EGFP-tropomodulin, respectively. Fig. S5 shows the speed of processive movement of the FH2 mutant of mDia1 in the cell peripheral area. Videos 1–10 show time-lapse images of EGFP-tagged probes in XTC cells. Online supplemental material is available at http://www.jcb.org/cgi/content/full/jcb.200604176/DC1.

We thank Roger Y. Tsien for mRFP1 cDNA, Kensaku Mizuno for human LIMK-1 cDNA, Timothy J. Mitchison and Goro Eguchi for critical reading of the manuscript, and James Monypenny for discussion and editing of the manuscript.

This work is supported, in part, by a Grant-in-Aid for Scientific Research on Priority Areas from the Ministry of Education, Culture, Sports, Science and Technology of Japan and by grants from PRESTO (Japan Science and Technology Agency), Uehara Memorial Foundation, Associazione Italiana Ricerca sul Cancro, Human Science Frontier Program (grant RGP0072/2003-C to G. Scita), and the European Community (VI Framework).

Submitted: 26 April 2006
Accepted: 20 November 2006

References

Abraham, V.C., V. Krishnamurthi, D.L. Taylor, and F. Lanni. 1999. The actin-based nanomachine at the leading edge of migrating cells. *Biophys. J.* 77:1721–1732.

Amann, K.J., and T.D. Pollard. 2001. Direct real-time observation of actin filament branching mediated by Arp2/3 complex using total internal reflection fluorescence microscopy. *Proc. Natl. Acad. Sci. USA*. 98:15009–15013.

Andrianantoandro, E., L. Blanchoin, D. Sept, J.A. McCammon, and T.D. Pollard. 2001. Kinetic mechanism of end-to-end annealing of actin filaments. *J. Mol. Biol.* 312:721–730.

Azuma, T., W. Witke, T.P. Stossel, J.H. Hartwig, and D.J. Kwiatkowski. 1998. Gelsolin is a downstream effector of rac for fibroblast motility. *EMBO J.* 17:1362–1370.

Bamburg, J.R. 1999. Proteins of the ADF/cofilin family: essential regulators of actin dynamics. *Annu. Rev. Cell Dev. Biol.* 15:185–230.

Barzik, M., T.I. Kotova, H.N. Higgs, L. Hazelwood, D. Hanein, F.B. Gertler, and D.A. Schafer. 2005. Ena/VASP proteins enhance actin polymerization in the presence of barbed end capping proteins. *J. Biol. Chem.* 280:28653–28662.

Bear, J.E., T.M. Svitkina, M. Krause, D.A. Schafer, J.J. Loureiro, G.A. Strasser, I.V. Maly, O.Y. Chaga, J.A. Cooper, G.G. Borisy, and F.B. Gertler. 2002. Antagonism between Ena/VASP proteins and actin filament capping regulates fibroblast motility. *Cell*. 109:509–521.

Bryce, N.S., G. Schevzov, V. Ferguson, J.M. Percival, J.J. Lin, F. Matsumura, J.R. Bamburg, P.L. Jeffrey, E.C. Hardeman, P. Gunning, and R.P. Weinberger. 2003. Specification of actin filament function and molecular composition by tropomyosin isoforms. *Mol. Biol. Cell*. 14:1002–1016.

Bubb, M.R., A.M. Senderowicz, E.A. Sausville, K.L. Duncan, and E.D. Korn. 1994. Jasplakinolide, a cytotoxic natural product, induces actin polymerization and competitively inhibits the binding of phalloidin to F-actin. *J. Biol. Chem.* 269:14869–14871.

Bubb, M.R., I. Spector, B.B. Beyer, and K.M. Fosen. 2000. Effects of jasplakinolide on the kinetics of actin polymerization. An explanation for certain in vivo observations. *J. Biol. Chem.* 275:5163–5170.

Caldwell, J.E., S.G. Heiss, V. Mermall, and J.A. Cooper. 1989. Effects of CapZ, an actin capping protein of muscle, on the polymerization of actin. *Biochemistry*. 28:8506–8514.

Campbell, R.E., O. Tour, A.E. Palmer, P.A. Steinbach, G.S. Baird, D.A. Zacharias, and R.Y. Tsien. 2002. A monomeric red fluorescent protein. *Proc. Natl. Acad. Sci. USA*. 99:7877–7882.

Carlier, M.F., D. Pantaloni, and E.D. Korn. 1984. Steady state length distribution of F-actin under controlled fragmentation and mechanism of length redistribution following fragmentation. *J. Biol. Chem.* 259:9987–9991.

Carlier, M.F., C. Le Clainche, S. Wiesner, and D. Pantaloni. 2003. Actin-based motility: from molecules to movement. *Bioessays*. 25:336–345.

Casella, J.F., and M.A. Torres. 1994. Interaction of Cap Z with actin. The NH2-terminal domains of the alpha 1 and beta subunits are not required for actin capping, and alpha 1 beta and alpha 2 beta heterodimers bind differentially to actin. *J. Biol. Chem.* 269:6992–6998.

Chan, A.Y., M. Bailly, N. Zebda, J.E. Segall, and J.S. Condeelis. 2000. Role of cofilin in epidermal growth factor-stimulated actin polymerization and lamellipod protrusion. *J. Cell Biol.* 148:531–542.

Croce, A., G. Cassata, A. Disanza, M.C. Gagliani, C. Tacchetti, M.G. Malabarba, M.F. Carlier, G. Scita, R. Baumeister, and P.P. Di Fiore. 2004. A novel actin barbed-end-capping activity in EPS-8 regulates apical morphogenesis in intestinal cells of *Caenorhabditis elegans*. *Nat. Cell Biol.* 6:1173–1179.

DiNubile, M.J., L. Cassimeris, M. Joyce, and S.H. Zigmond. 1995. Actin filament barbed-end capping activity in neutrophil lysates: the role of capping protein-beta 2. *Mol. Biol. Cell*. 6:1659–1671.

Disanza, A., M.F. Carlier, T.E. Stradal, D. Didry, E. Frittoli, S. Confalonieri, A. Croce, J. Wehland, P.P. Di Fiore, and G. Scita. 2004. Eps8 controls actin-based motility by capping the barbed ends of actin filaments. *Nat. Cell Biol.* 6:1180–1188.

Falck, S., V.O. Paavilainen, M.A. Wear, J.G. Grossmann, J.A. Cooper, and P. Lappalainen. 2004. Biological role and structural mechanism of twinfilin-capping protein interaction. *EMBO J.* 23:3010–3019.

Fujiwara, I., S. Suetsugu, S. Uemura, T. Takenawa, and S. Ishiwata. 2002. Visualization and force measurement of branching by Arp2/3 complex and N-WASP in actin filament. *Biochem. Biophys. Res. Commun.* 293:1550–1555.

Gournier, H., E.D. Goley, H. Niederstrasser, T. Trinh, and M.D. Welch. 2001. Reconstitution of human Arp2/3 complex reveals critical roles of individual subunits in complex structure and activity. *Mol. Cell*. 8:1041–1052.

Helfer, E., E.M. Nevalainen, P. Naumanen, S. Romero, D. Didry, D. Pantaloni, P. Lappalainen, and M.F. Carlier. 2006. Mammalian twinfilin sequesters ADP-G-actin and caps filament barbed ends: implications in motility. *EMBO J.* 25:1184–1195.

Higashida, C., T. Miyoshi, A. Fujita, F. Oceguera-Yanez, J. Monypenny, Y. Andou, S. Narumiya, and N. Watanabe. 2004. Actin polymerization-driven molecular movement of mDia1 in living cells. *Science*. 303:2007–2010.

Hotulainen, P., E. Paunola, M.K. Vartiainen, and P. Lappalainen. 2005. Actin-depolymerizing factor and cofilin-1 play overlapping roles in promoting rapid F-actin depolymerization in mammalian nonmuscle cells. *Mol. Biol. Cell*. 16:649–664.

Huang, M., M. Pring, C. Yang, M. Taoka, and S.H. Zigmond. 2005. Presence of a novel inhibitor of capping protein in neutrophil extract. *Cell Motil. Cytoskeleton*. 62:232–243.

Hug, C., P.Y. Jay, I. Reddy, J.G. McNally, P.C. Bridgman, E.L. Elson, and J.A. Cooper. 1995. Capping protein levels influence actin assembly and cell motility in *Dictyostelium*. *Cell*. 81:591–600.

Kovar, D.R., E.S. Harris, R. Mahaffy, H.N. Higgs, and T.D. Pollard. 2006. Control of the assembly of ATP- and ADP-actin by formins and profilin. *Cell*. 124:423–435.

Mejillano, M.R., S. Kojima, D.A. Applewhite, F.B. Gertler, T.M. Svitkina, and G.G. Borisy. 2004. Lamellipodial versus filopodial mode of the actin nanomachinery: pivotal role of the filament barbed end. *Cell*. 118:363–373.

Mullins, R.D., W.F. Stafford, and T.D. Pollard. 1997. Structure, subunit topology, and actin-binding activity of the Arp2/3 complex from *Acanthamoeba*. *J. Cell Biol.* 136:331–343.

Mullins, R.D., J.A. Heuser, and T.D. Pollard. 1998. The interaction of Arp2/3 complex with actin: nucleation, high affinity pointed end capping, and formation of branching networks of filaments. *Proc. Natl. Acad. Sci. USA*. 95:6181–6186.

Nagata-Ohashi, K., Y. Ohta, K. Goto, S. Chiba, R. Mori, M. Nishita, K. Ohashi, K. Kousaka, A. Iwamatsu, R. Niwa, et al. 2004. A pathway of neuregulin-induced activation of cofilin-phosphatase Slingshot and cofilin in lamellipodia. *J. Cell Biol.* 165:465–471.

Nakagawa, H., H. Miki, M. Ito, K. Ohashi, T. Takenawa, and S. Miyamoto. 2001. N-WASP, WAVE and Mena play different roles in the organization of actin cytoskeleton in lamellipodia. *J. Cell Sci.* 114:1555–1565.

Nakaoka, Y., and M. Kasai. 1969. Behaviour of sonicated actin polymers: adenosine triphosphate splitting and polymerization. *J. Mol. Biol.* 44:319–332.

Pollard, T.D., and G.G. Borisy. 2003. Cellular motility driven by assembly and disassembly of actin filaments. *Cell*. 112:453–465.

Rogers, S.L., U. Wiedemann, N. Stuurman, and R.D. Vale. 2003. Molecular requirements for actin-based lamella formation in *Drosophila* S2 cells. *J. Cell Biol.* 162:1079–1088.

Schafer, D.A., Y.O. Korshunova, T.A. Schroer, and J.A. Cooper. 1994. Differential localization and sequence analysis of capping protein β-subunit isoforms of vertebrates. *J. Cell Biol.* 127:453–465.

Schafer, D.A., P.B. Jennings, and J.A. Cooper. 1996. Dynamics of capping protein and actin assembly in vitro: uncapping barbed ends by polyphosphoinositides. *J. Cell Biol.* 135:169–179.

Schafer, D.A., M.D. Welch, L.M. Machesky, P.C. Bridgman, S.M. Meyer, and J.A. Cooper. 1998. Visualization and molecular analysis of actin assembly in living cells. *J. Cell Biol.* 143:1919–1930.

Scita, G., J. Nordstrom, R. Carbone, P. Tenca, G. Giardina, S. Gutkind, M. Bjarnegard, C. Betsholtz, and P.P. Di Fiore. 1999. EPS8 and E3B1 transduce signals from Ras to Rac. *Nature*. 401:290–293.

Scita, G., P. Tenca, L.B. Areces, A. Tocchetti, E. Frittoli, G. Giardina, I. Ponzanelli, P. Sini, M. Innocenti, and P.P. Di Fiore. 2001. An effector region in Eps8 is responsible for the activation of the Rac-specific GEF activity of Sos-1 and for the proper localization of the Rac-based actin-polymerizing machine. *J. Cell Biol.* 154:1031–1044.

Small, J.V., G. Isenberg, and J.E. Celis. 1978. Polarity of actin at the leading edge of cultured cells. *Nature*. 272:638–639.

Small, J.V., M. Herzog, and K. Anderson. 1995. Actin filament organization in the fish keratocyte lamellipodium. *J. Cell Biol.* 129:1275–1286.

Svitkina, T.M., and G.G. Borisy. 1999. Arp2/3 complex and actin depolymerizing factor/cofilin in dendritic organization and treadmilling of actin filament array in lamellipodia. *J. Cell Biol.* 145:1009–1026.

Theriot, J.A., and T.J. Mitchison. 1991. Actin microfilament dynamics in locomoting cells. *Nature*. 352:126–131.

Watanabe, N., and T.J. Mitchison. 2002. Single-molecule speckle analysis of actin filament turnover in lamellipodia. *Science*. 295:1083–1086.

Wear, M.A., and J.A. Cooper. 2004. Capping protein: new insights into mechanism and regulation. *Trends Biochem. Sci.* 29:418–428.

Weber, A., C.R. Pennise, G.G. Babcock, and V.M. Fowler. 1994. Tropomodulin caps the pointed ends of actin filaments. *J. Cell Biol.* 127:1627–1635.

Welch, M.D., A.H. DePace, S. Verma, A. Iwamatsu, and T.J. Mitchison. 1997. The human Arp2/3 complex is composed of evolutionarily conserved subunits and is localized to cellular regions of dynamic actin filament assembly. *J. Cell Biol.* 138:375–384.

Welch, M.D., J. Rosenblatt, J. Skoble, D.A. Portnoy, and T.J. Mitchison. 1998. Interaction of human Arp2/3 complex and the *Listeria monocytogenes* ActA protein in actin filament nucleation. *Science*. 281:105–108.

Witke, W., A.H. Sharpe, J.H. Hartwig, T. Azuma, T.P. Stossel, and D.J. Kwiatkowski. 1995. Hemostatic, inflammatory, and fibroblast responses are blunted in mice lacking gelsolin. *Cell*. 81:41–51.

Yang, N., O. Higuchi, K. Ohashi, K. Nagata, A. Wada, K. Kangawa, E. Nishida, and K. Mizuno. 1998. Cofilin phosphorylation by LIM-kinase 1 and its role in Rac-mediated actin reorganization. *Nature*. 393:809–812.

Yang, C., M. Pring, M.A. Wear, M. Huang, J.A. Cooper, T.M. Svitkina, and S.H. Zigmond. 2005. Mammalian CARMIL inhibits actin filament capping by capping protein. *Dev. Cell*. 9:209–221.